

INFLUENCE OF THE LOW ENERGIES RESONANCES ON THE $n^{11}\text{B}$ CAPTURE REACTION RATE

Dubovichenko S.B.^{1,2*}, **Burkova N.A.**², **Dzhazairov-Kakhramanov A.V.**^{1†},
Tkachenko A.S.^{1,2}

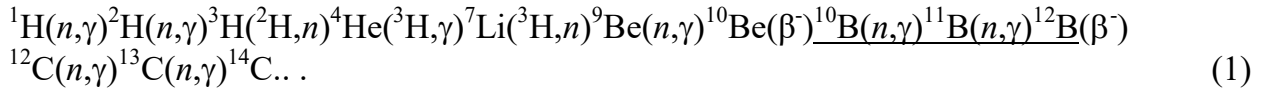
¹*Fesenkov Astrophysical Institute “NCSRT” ASA MDASI RK, 050020, Almaty, Kazakhstan*

²*al-Farabi Kazakh National University, 050040, Almaty, Kazakhstan*

Within the framework of the modified potential cluster model (MPCM) with a classification of orbital states according to Young schemes (diagrams), the possibility of describing experimental data for total cross sections of radiative $n^{11}\text{B}$ capture on the ground state (GS) of ^{12}B nucleus at energies from 10 meV (1 meV = 10^{-3} eV) to 7 MeV was considered. It was shown that, taking into account only the $E1$ -transition from the S -state of $n^{11}\text{B}$ scattering to the ground state of the ^{12}B nucleus in the $n^{11}\text{B}$ channel, it is quite possible to explain the magnitude of the known experimental cross sections at energies from 25.3 meV to 70 keV. Further, on the basis of the total cross sections from 10 meV to 7 MeV, but excluding resonances above 5 MeV, the reaction rate is calculated in the temperature range from 0.01 to 10.0 T_9 . It is shown that the inclusion of low-lying resonant states makes a significant contribution to the reaction rate, starting already with temperatures of 0.2–0.3 T_9 .

Introduction

In recent years, the role of *short-lived isotopes* that are included in various chains of the synthesis of heavier elements in astrophysical processes has been actively discussed. This role is noticeable both in the processes of primordial nucleosynthesis and in nuclear processes during supernova explosions. A well-known yield on carbon components is proposed as a sequence of processes [1, 2, 3, 4, 5]



Most recently, we have considered reactions of the neutrons radiative capture neutrons on ^{10}Be [6] and ^{10}B [7] nuclei, as well as the proton capture on ^7Be [8] nuclei. Continuing to study the processes of radiation capture in the framework of the modified potential cluster model (MPCM) [9, 10] we now consider the reaction of radiation capture $n^{11}\text{B} \rightarrow {}^{12}\text{B}$ at thermal and astrophysical energies. In the present research, we will use the new data on the spectra of the ^{11}B nucleus from [11], compared with our previous scientific papers [12], where the results of the earlier review [13] were.

In addition, for the first time, resonances in the scattering phase shifts of the initial particles of the input channel are taken into account. In other words, the potentials of $n^{11}\text{B}$ interactions for scattering processes now describe the main resonance states of the final nucleus ^{12}B , which are considered in the $n^{11}\text{B}$ channel at the positive energy. Despite the fact that there are no direct experimental measurements of total cross sections at energies greater than 70 keV [11, 14], in the calculations of the $n^{11}\text{B} \rightarrow \gamma^{12}\text{B}$ reaction cross sections we took into account resonant states up to 5 MeV, which are now confirmed by new data on excitation energies and widths of the corresponding levels [11].

The $n^{11}\text{B} \rightarrow \gamma^{12}\text{B}$ reaction that we considered was studied earlier in [15], where the thermal cross section for neutron capture equal to 5.5 μb [16] was used to construct the

* Corresponding author: dubovichenko@gmail.com.

† Corresponding author: albert-j@yandex.kz.

$n^{11}\text{B}$ interaction potentials. At the same time, in this paper we will use newer data from [17], where the value = 9.09 (10) μb is given.

Our calculations, in essence, are predictive and evaluative for substantiating and conducting new experiments on the $n^{11}\text{B}$ capture. Such results may also initiate a significant reassessment of the synthesis rate of the ^{12}B isotope at temperatures above $0.2 T_9$. This, in turn, will allow assessing how much the balance of elements synthesized in the chain (1) can change, which is relevant for describing the evolution of astrophysical objects.

Calculation methods

In the last half century for the description of astrophysical reactions the microscopic model has become a successful direction – the resonant groups method (RGM) (see, for example, [18, 19]), and also related models, for example, the generator coordinate method (GCM, see, in particular, [20]) or the algebraic version of the RGM (see, for example, [21] and references therein). However, the possibilities of simple potential two-cluster models (PCM) have not yet been fully investigated, especially if they use the concept of forbidden states (FSs) [22, 23], and also directly take into account the behavior of the phase shifts of elastic scattering of interacting particles at low energies – such a variant of the model can be called modified PCM with FSs or MPCM [9, 10].

In particular, in our previous works [6-10, 24, 25, 26, 27] (see also the references in the review [24]), the possibility of describing the basic characteristics of bound states (BSs) of some nuclei and astrophysical S -factors or total cross sections of radiation capture for more than 30 reactions of the type of radiation capture at thermal and astrophysical energies is shown. Calculations of these processes are made on the basis of the MPCM with the classification of states according to Young schemes (diagrams), which leads to forbidden, in some cases, states. The definite success of the MPCM can be explained by the fact that the potentials of intercluster interaction are built not only on the basis of known elastic scattering phase shifts, but with allowance for the classification of cluster states according to Young schemes (diagrams) [22]. In addition, the potentials of bound or ground states (GSs) with FSs in some partial waves are based on the description of the binding energy, radii and asymptotic constants (ACs) of the final nucleus in the cluster channel under consideration. Further, such potentials allow one to perform calculations of certain characteristics of the interaction of the considered particles in the processes of elastic scattering and capture reactions [9, 10].

$$\sigma_c(NJ, J_f) = \frac{8\pi K e^2}{\hbar^2 q^3} \frac{\mu}{(2S_1 + 1)(2S_2 + 1)} \frac{J + 1}{J[(2J + 1)!!]^2} A_J^2(NJ, K) \sum_{L_i, J_i} P_J^2(NJ, J_f, J_i) I_J^2(J_f, J_i)$$

where σ is the total cross section of the radiative capture process, μ is the reduced mass of particles in the input channel, q is the wave number of particles in the input channel, S_1 and S_2 are the spins of particles in the input channel, K and J is the wave number and the angular momentum of the γ -quantum in the output channel, respectively, NJ are the E or M transitions of the J -th multipolarity from the initial J_i state of two particles in the continuous spectrum to the final, bounded J_f state of the nucleus in a two-cluster channel.

For electric orbital $EJ(L)$ -transitions, the values of P_J , A_J and I_J have the form (see, for example, [28])

$$P_J^2(EJ, J_f, J_i) = \delta_{S_i S_f} \left[(2J+1)(2L_i+1)(2J_i+1)(2J_f+1) \right] (L_i 0 J 0 | L_f 0)^2 \left\{ \begin{matrix} L_i & S & J_i \\ J_f & J & L_f \end{matrix} \right\}^2 \quad (2)$$

$$A_J(EJ, K) = K^J \mu^J \left(\frac{Z_1}{m_1^J} + (-1)^J \frac{Z_2}{m_2^J} \right), \quad I_J(J_f, J_i) = \langle \chi_f | r^J | \chi_i \rangle.$$

Here L_i, L_f, J_i, J_f are the orbital and total momenta of particles of the initial (i) and final (f) channels, m_1, m_2, Z_1, Z_2 are the masses and charges of the particles of the initial channel, I_J is the integral over the wave functions of the initial χ_i and the final χ_f state of clusters, as functions of the relative motion of clusters with the intercluster distance r .

To consider the magnetic $MI(S)$ -transition, due to the spin part of the magnetic operator, we use the following expressions [9, 10]

$$P_1^2(M1, J_f, J_i) = \delta_{S_i S_f} \delta_{L_i L_f} \left[S(S+1)(2S+1)(2J_i+1)(2J_f+1) \right] \left\{ \begin{matrix} S & L & J_i \\ J_f & 1 & S \end{matrix} \right\}^2, \quad (3)$$

$$A_1(M1, K) = i \frac{e\hbar}{m_0 c} K \sqrt{3} \left[\mu_1 \frac{m_2}{m} - \mu_2 \frac{m_1}{m} \right], \quad I_J(J_f, J_i) = \langle \chi_f | r^{J-1} | \chi_i \rangle, \quad J = 1.$$

Here m is the mass of the nucleus, μ_1 and μ_2 are the magnetic momenta of the clusters, the values of which are taken from the databases [31, 32], namely $\mu_n = -1.91304272\mu_0$ and $\mu(^{11}\text{B}) = 2.6887\mu_0$.

In the calculations we used the following values of particle masses $m_n = 1.00866491597$ a.m.u. [31], $m(^{11}\text{B}) = 11.0093052$ a.m.u. [32], and the constant \hbar^2/m_0 was taken to be 41.4686 MeV·fm², where m_0 is a.m.u. The Coulomb parameter $\eta = \mu Z_1 Z_2 e^2 / (q \hbar^2)$ has the form $\eta = 3.44476 \cdot 10^{-2} \cdot Z_1 Z_2 \mu / q$, where q is the wave number in fm⁻¹. The Coulomb potential at $R_{\text{coul}} = 0$ was written as $V_{\text{coul}}(\text{MeV}) = 1.439975 \cdot Z_1 Z_2 / r$, where r is the distance between particles in fm. Methods for calculating of other quantities in the MPCM framework, for example, root-mean-square mass and charge radii or binding energy, which are discussed further, are given, for example, in our works [9, 10, 30].

Potential constructing in the MPCM

Let us consider in more detail the procedure for constructing the intercluster partial potentials used here (in this case, the interaction potentials of the neutron and the target nucleus) for a given orbital angular momentum L and other quantum numbers, determining the criteria and the algorithm of finding the parameters and indicating their errors and ambiguities.

First of all, parameters of potentials of bound states, for example, GS, should be determined, which, for a given number of bound states, are fixed quite uniquely by the binding energy, nuclear radius and AC in the channel under consideration. When constructing partial interaction potentials in MPCM, it is considered that they depend not only on the orbital momentum L , but also on the total spin S and the total momentum J of the considered system of nuclear particles. Here and in our previous works [9, 10], we use Gaussian interaction potentials that depend on JLS quantum numbers, as well as on Young schemes (diagrams).

In other words, for the different JLS momenta we will have different values of the parameters of the partial potential. Since $E1$ or $M1$ -transitions between different $(2S+1)L_J$ states in the continuous and discrete spectra are usually considered, the potentials of these states will also be different [24, 27]. Note once again that we use MPCM for our calculations and one of its modifications consists in the explicit dependence of the potentials used on Young's schemes $\{f\}$ and taking into account, in some cases, the mixing of scattering states according to Young's schemes [9, 10, 22]. Taking into account the explicit dependence of the interaction potentials on Young schemes makes it possible to use different potentials in scattering and discrete spectrum states if they depend on a different set of such schemes, as was the case, for example, in the N^2H system [22, 27].

The accuracy with which the parameters of the potential of the BSs are determined in this way is connected, first of all, with the accuracy of the AC. This potential does not contain any other ambiguities, since the classification of states according to Young's schemes makes it possible to unambiguously fix the number of bounded forbidden and allowed states in a given partial wave. Their number fully determines its depth, and the width of the potential depends entirely on the size of the AC. The principles for determining the number of FSs and allowed states (ASs) in a given partial wave based on Young's schemes for the $n^{11}B$ system considered here are given below. They are described in more detail in [22, 27].

It should be noted here that calculations of the charge radius in any model contain model errors. In any model, the magnitude of such a radius depends on the integral of the model wave functions (WF), i.e. model errors of such functions are simply summarized. At the same time, AC values are determined by the asymptotic behavior of model WFs at one point and, apparently, contain a significantly smaller error. Therefore, the potentials of the BSs and GSs are constructed so that, first of all, they agree as much as possible with the values of AC, obtained on the basis of independent methods, which allow extracting AC from experimental data (see, for example, [33]).

The intercluster potential of the nonresonant process of scattering based on the phase shift of scattering for a given number of BSs allowed and forbidden in the considered partial wave is also can be constructed quite unambiguously. The accuracy of determining the parameters of such a potential depends, first of all, on the accuracy of extracting the scattering phase shifts from the experimental data and can reach 20–30%. Here, the potential does not contain ambiguities, since the classification of states according to Young's schemes makes it possible to unambiguously fix the number of BSs, which completely determines its depth, and the potential width at a given depth is determined by the shape of the scattering phase shifts.

When constructing a nonresonant scattering potential from the data on the spectra of the nucleus, it is difficult to estimate the accuracy of finding its parameters even for a given number of BSs, although it can be expected that it does not exceed the error in the previous case. Such a potential, as is usually assumed for the energy range up to 1-3 MeV, should lead to a scattering phase shift close to zero or give a smoothly falling form of the phase shift, since the resonance levels in the spectra of the nucleus are absent.

In the analysis of the resonance scattering, when in the considered partial wave at energies up to 1-3 MeV there is a relatively narrow resonance with a width of the order of 10 - 50 keV, for a given number of BSs, the potential is constructed distinctly. For a given number of BSs, its depth is completely fixed by the resonant energy of the level, and the width of the potential is determined by the width of this resonance. The error of its parameters usually does not exceed the error of determining the width of this level and

is approximately 5 - 10%. Moreover, this applies to the construction of the partial potential from the resonant phase shifts of scattering and the determination of its parameters from the resonance in the spectra of the nucleus.

As a result, all these potentials do not contain ambiguities inherent in optical models [34], and as was shown [9, 10] allow us to describe correctly the total cross sections of many processes of radiative capture. The potentials of the BSs should correctly describe the known values of the AC, which is associated with the asymptotic normalization coefficient (ANC) of the A_{NC} usually extracted from the experiment as follows [33]

$$A_{NC}^2 = S_f \cdot C^2 \quad (4)$$

where S_f is the spectroscopic factor of the channel and C is the dimensional AC, expressed in $\text{Fm}^{-1/2}$ and determined from the relation

$$\chi_L(r) = C \cdot W_{-\eta L+1/2}(2k_0 r). \quad (5)$$

C is related to the dimensionless AC C_w [35], used by us, as follows: $C = \sqrt{2k_0} C_w$, and the dimensionless constant C_w can be defined by the expression [35]

$$\chi_L(r) = \sqrt{2k_0} \cdot C_w \cdot W_{-\eta L+1/2}(2k_0 r), \quad (6)$$

where $\chi_L(r)$ is the numerical wave function of the bound state obtained from the solution of the radial Schrödinger equation and normalized to one, $W_{-\eta L+1/2}$ is the Whittaker function of the bound state, which determines the asymptotic behavior of the WF and is a solution of the same equation without nuclear potential, i.e. at large distances $r = R$, k_0 is the wave number due to the channel binding energy, η is the Coulomb parameter, and L is the orbital momentum of this bound state.

State structure of the $n^{11}\text{B}$ system

We do not have complete tables of products of Young schemes for a system with more than eight particles [36], which we used earlier for similar calculations [9, 10]. Therefore, the results obtained below should be considered only as a qualitative assessment of possible orbital symmetries in the ground state of the ^{12}B core for the $n^{11}\text{B}$ channel. At the same time, based on this classification it was possible to adequately explain the available experimental data on the radiative capture of nucleons and light clusters on $1p$ -shell nuclei [9, 10]. Therefore, here we will use the classification of cluster states according to orbital symmetries, which leads us to a certain number of FSs and ASs in partial intercluster potentials, and, therefore, to a certain number of nodes of the wave function of the relative motion of clusters - in this case, the neutron and ^{11}B nucleus.

Further assume that for ^{11}B (spin and isospin of the ^{11}B nucleus have the values $J^\pi, T = 3/2^-, 1/2$ [11]) we can accept the Young orbital scheme in the form $\{443\}$, therefore for the $n^{11}\text{B}$ system we have $\{1\} \times \{443\} \rightarrow \{543\} + \{444\} + \{4431\}$ [22,36]. The first of the schemes obtained is compatible with the orbital momenta $L = 1, 2, 3, 4$ and is forbidden, since there cannot be five nucleons in the s -shell [22, 27], the second $\{444\}$ scheme

seems to be allowed and compatible with the orbital momentum $L = 0, 2, 4$, and the third one $\{4431\}$, also allowed, is compatible with $L = 1, 2, 3$ [23].

Thus, limited to only the lowest partial waves with the orbital angular momentum $L = 0, 1, 2$, we can say that for the $n^{11}\text{B}$ system, only the AS for the $\{444\}$ scheme is present in the S -wave potential. In P -waves, there is a forbidden state at $\{543\}$ and allowed at $\{4431\}$. In particular, in the 3P_1 -wave with $\{4431\}$ AS corresponds the GS of ${}^{12}\text{B}$ with momenta $J^\pi, T = 1^+, 1$ at the binding energy of the $n^{11}\text{B}$ -system equals 3.370 MeV [11]. For D -waves, we have FS with the scheme $\{543\}$ and AS with $\{4431\} + \{444\}$. For F -waves, we have FS with the scheme $\{543\}$ and AS with $\{4431\}$. These ASs for the scattering potentials may be in the continuous spectrum and not be related. The methods used to determination the FSs or ASs allow us to determine their presence in a certain partial wave, but for the scattering states it is not possible to determine whether such a state will be bound. Therefore, for definiteness, we will further assume that the scattering states have only lower levels bound, whether they are allowed or forbidden.

If for the ${}^{11}\text{B}$ nucleus we accept the Young orbital scheme in the form $\{4421\}$, then for the $n^{11}\text{B}$ system we have $\{1\} \times \{4421\} = \{5421\} + \{4431\} + \{4422\}$. The first scheme is forbidden - it corresponds to the orbital momenta $L = 1, 2, 3$, and the second one is allowed for the momenta $L = 1, 2, 3$, the third scheme is also allowed and has $L = 0, 2$. Thus considering only the waves with the orbital momentum $L = 0, 1, 2$, we can assume that for the $n^{11}\text{B}$ system only the AS is present in the potential of the 3S_1 wave. In each 3P wave there is a forbidden $\{5421\}$ and allowed $\{4431\}$ states. For D -waves, we have FS with the $\{5421\}$ scheme and the AS for $\{4431\} + \{4422\}$, and for F -waves, we have the FS with the $\{5421\}$ scheme and the AS for $\{4431\}$. ASs for scattering potentials can also be in the continuous spectrum, and not be bound. From this classification it is clear that in this case, the presence and number of bound FSs and ASs in these partial waves, as compared with the previous case, remains the same, although now they are compared with the other orbital Young schemes.

Some $n^{11}\text{B}$ -scattering states and BSs can be mixed along the channel spin with a value of 1 and 2. Therefore, both spin states 3P_1 and 5P_1 can contribute to the WF of the GS, and the GS should be considered as a ${}^{3+5}P_1$ -mixture. This model does not allow to isolate states with $S = 1$ and 2 in the WF, so the GS function is ${}^{3+5}P_1$ -level and is obtained by solving the Schrödinger equation with a given GS potential. A similar situation existed, for example, with $n^{15}\text{N}$ or $n^7\text{Li}$ capture, when the GS wave function was represented by a mixture of ${}^{3+5}P_2$ waves [9, 10, 37, 38, 39].

Possible transitions in the $n^{11}\text{B}$ system

Since the GS of the ${}^{12}\text{B}$ nucleus here correlates the ${}^{3+5}P_1$ level, we can consider $E1$ transitions from nonresonant at low energies of the 3S_1 and 5S_2 $n^{11}\text{B}$ scattering waves to the different components of the WF of the GS of the ${}^{12}\text{B}$ nucleus in the $n^{11}\text{B}$ channel

$$1. \quad \begin{array}{l} {}^3S_1 \xrightarrow{E1} {}^3P_1 \\ {}^5S_2 \xrightarrow{E1} {}^5P_1 \end{array}.$$

The cross sections of this process can be written as a sum

$$\sigma(E1) = \sigma(^3S_1 \rightarrow ^3P_1) + \sigma(^5S_2 \rightarrow ^5P_1)$$

since the transitions originate from different partial scattering waves on the same GS of the ^{12}B nucleus, to which the spin-mixed $^{3+5}P_1$ WF is matched – only the P_J coefficients in the expression for the cross sections (2) and (3) are different.

Now consider the ^{12}B nucleus excited states (ESs) that are bound in the $n^{11}\text{B}$ channel

1. At an excitation energy of 0.95314 (60) MeV or -2.41686 (60) MeV [11] respect to the threshold of the $n^{11}\text{B}$ channel, there is a first excited (FES) but bound in this channel state with the momentum is $J^\pi = 2^+$, which can be compared with the $^{3+5}P_2$ -wave with the bound FS.

2. The second excited state (SES) with an excitation energy of 1.67365 (60) MeV [13] relative to the GS or -1.69635 (60) MeV relative to the threshold of the $n^{11}\text{B}$ channel has $J^\pi = 2^-$ and it can be compared with the 5S_2 wave without a bound FS. In this case, a $^{3+5}D_2$ -wave is also possible with the bound FS.

3. The third excited state (TES) state with an excitation energy of 2.6208 (12) MeV [11] or -0.7492 (12) MeV relative to the threshold of the $n^{11}\text{B}$ channel has $J^\pi = 1^-$ and can be compared with the triplet 3S_1 -wave without the forbidden BS. In this case, a $^{3+5}D_1$ -wave with a FS is also possible.

4. The fourth excited state (FES) with an excitation energy of 2.723 (11) MeV or -0.647 (11) MeV [11] with respect to the threshold of the $n^{11}\text{B}$ channel has $J^\pi = 0^+$ and can be compared with a triplet 3P_0 -wave with a bound FS.

Further, we construct the potentials of the last three ESs, which will be used to describe the scattering processes in these partial waves that do not contain resonances. However, there is a resonance in the $^{3+5}P_2$ scattering wave, and to build a $^{3+5}P_2$ -potential, which has both the resonance and the first bound ES with the Gaussian form of potential parametrization used by us, is not possible. Therefore, in the future, when considering the capture on the first ES, different potentials for the discrete and continuous spectrum will be used. Here only $^{3+5}P_2$ -potential for the resonant scattering wave will be obtained.

In addition to the excited states, there are several resonant levels (RLs), i.e. states at positive energies relative to the threshold of the $n^{11}\text{B}$ -channel (italics indicate the levels that are present in the spectra, but are not considered by us for various reasons)

1. The first resonant state (1RL) of the ^{12}B nucleus in the $n^{11}\text{B}$ -channel is at an excitation energy of 3.3891 (16) MeV or $E_n = 20.8$ (5) keV, and has a width less than 1.4 keV in the c.m. and momentum $J^\pi = 3^-$ (see Table 12.10 in [11]) - it can be compared with the $^{3+5}D_3$ scattering wave with the forbidden bound state. We will not consider it, since it is impossible for it to have E1 or M1 transitions to the GS $^{3+5}P_1$.

2. The second resonant state (2RL) has energy $E_n = 430$ (10) keV - its width in the c.m. equal to 37 (5) keV and the momentum $J^\pi = 2^+$ [11]. Therefore, it can be compared with the $^{3+5}P_2$ scattering wave with the bound FS and for it M1 transitions to the GS $^{3+5}P_1$ are possible.

3. The third resonant state (3RL) is at energy $E_n = 1027$ (11) keV with a small width equal to 9 (4) keV in the c.m. and the momentum $J^\pi = 1^-$ [11] - it can be compared with the 3S_1 without the FS or $^{3+5}D_1$ scattering wave with the bound FS and for it E1 transitions to the GS $^{3+5}P_1$ are possible.

4. The fourth resonant state (4RL) is at energy $E_n = 1.19$ MeV with an unknown, but large width and momentum 2^- (see table 12.10 from [11]) - it can be compared to 5S_2 or $^{3+5}D_2$ scattering wave and for it $E1$ transitions to the GS $^{3+5}P_1$ are possible. However, we will not consider these transitions due to the unknown width.

5. The fifth resonance (5RL) has energy $E_n = 1.280$ (20) MeV with a width of 130 (20) keV in the c.m. and the momentum 4^- [11]. We will not consider it, because here the $E1$ or $M1$ transitions to the GS are impossible.

6. The sixth resonance (6RL) with $E_n = 1.780$ (20) MeV with a width 60 (20) keV in the c.m. and momentum $J^\pi = 1^+$ can be compared with the $^{+5}P_1$ scattering wave with the bound FS (see Table 12.10 [11]) and $M1$ transitions to the GS $^{3+5}P_1$ are possible for it. This state can be attributed also to the 5F_1 -wave with the FS, but then only the $E2$ -transition to the GS is possible. For it, we will build the resonance potential and determine the contribution of this process to the total capture cross sections.

7. The seventh resonance (7RL) at $E_n = 2.450$ (20) MeV with a width 110 (40) keV in the c.m. and the momentum $J^\pi = 3^+$ can be compared with either the 5P_3 or $^{3+5}F_3$ scattering waves (see Table 12.10 from [11]). We will consider it, and determine the contribution of this an $E2$ -process to the total capture on the GS cross sections.

8. The eighth resonance (8RL) at $E_n = 2.580$ (20) MeV with a width 55 (20) keV in the c.m. and the momentum $J^\pi = 3^-$ can be compared with the $^{3+5}D_3$ scattering wave (see Table 12.10 from [11]) and we will not consider it, since only the $M2$ process is possible here.

9. The ninth resonance (9RL) with $E_n = 2.9$ MeV with unknown width and momentum $J^\pi = 1^-$ can be compared with the 3S_1 scattering wave without FS (see table 12.10 from [11]) and can lead to $E1$ transitions to the GS. However, we will not consider it because of the unknown width.

10. The tenth resonance (10RL) at $E_n = 3.5$ MeV with a width of 140 keV and a momentum $J^\pi = 1^+$ can be compared with the $^{3+5}P_1$ scattering wave with the bound FS (see Table 12.10 from [11]) and can lead to $M1$ -transitions on the GS. This state can be also attributed to the 5F_1 -wave with the FS, but then only the $E2$ -transition to the GS is possible. For it, we build a resonant potential and determine the contribution of this process to the total capture cross sections.

11. Next comes the resonance (11RL) at a neutron energy of 4.03 MeV with an unknown width and momentum 1^- . It can be compared with the 3S_1 -wave without the FS, and $E1$ -transitions to the GS $^{3+5}P_1$ are possible for it. We will not consider it because of the unknown width.

12. The next resonance (12RL) is at an energy of 4.55 MeV with a width of less than 14 keV in the c.m. and an unknown momentum. However, we will not consider it because of the unknown momentum.

13. Next is the resonance state (13RL) with a neutron energy of 4.70 MeV, a width of 45 keV in the c.m. and a momentum 2^- . It can be compared with the 5S_2 -wave without the FS, and $E1$ transitions to the GS $^{3+5}P_1$ are possible for it. In this case, a $^{3+5}D_2$ -wave with the FS is also possible, which allows for an $E1$ transition to the GS.

14. Resonance state (14RL) at 4.80 MeV energy with a width of 90 keV in the c.m. has a momentum 1^- . It can be compared with the 3S_1 -wave without the FS, and $E1$ transitions to the GS $^{3+5}P_1$ are possible for it. In this case, the $^{3+5}D_1$ -wave with the FS is also possible, which allows for the $E1$ -transition to the GS.

15. Higher states have not yet been studied in a detail [11], and we will not consider them. As a result, the influence of 7 resonances at energies up to $E_n = 5$ MeV can be con-

sidered - these are resonances number 2, 3, 6, 7, 10, 13 and 14. The rest have no either known width or momentum, so it is impossible for them to build unambiguous potentials, as is done for the remaining resonances. Some resonances, for example, the first (1RL), do not lead to $E1$ or $M1$ -transitions and will not be considered. In addition, it will be shown that when considering the $E2$ transitions for resonances 6, 7 and 10, if we accept F -waves for them, the cross sections obtained are several orders of magnitude smaller than the cross sections for the $E1$ and $M1$ -transitions.

As it was shown, states 3, 13, and 14 coincide with the second, third, and fourth ESs, but it is impossible to build S -potentials that would have a bound AS coinciding with one of the ESs and having resonance with the observed excitation energy. Therefore, we construct these resonance potentials so that they correspond to D -waves with the FS and have a resonance at the required energy with the required width. Based on the given above information about the ESs and RLs, it is possible to consider other $E1$ -transitions from non-resonant in the considered region of the energy S and D -scattering waves, as well as $M1$ -processes from the resonant $^{3+5}P_2$ -wave and non-resonant P_0 -wave. As already mentioned, for the S -waves and P_0 scattering wave we will use the potentials of the second, third and fourth ESs, and for 2RL in the P_2 -wave potential, which has a resonance and a bound FS, and does not coincide with the FES. As a result of the analysis of these RLs, the transitions that are listed in Table 1 will be further considered.

Table 1. A list of possible transitions from the initial $\{(^{2S+1})L_J\}_i$ state to the different components of the WF $\{(^{2S+1})L_J\}_f$ of the ^{12}B nucleus GS in $n^{11}\text{B}$ -capture and the parameters of Gaussian potentials, which are defined below, for the initial states. The value of P^2 determines the coefficient in the cross sections (2) and (3).

№	$\{(^{2S+1})L_J\}_i$ for the initial $n^{11}\text{B}$ -channel	Transition type	$\{(^{2S+1})L_J\}_f$ for the final $n^{11}\text{B}$ -channel	P^2 (to define the cross sections)	V_0 , MэВ	α , fm ⁻²
1.	3S_1 - nonresonant scattering wave.	$E1$	3P_1	3	5.61427	0.04
2.	5S_2 - nonresonant scattering wave.	$E1$	5P_1	3	13.56295 (6.70125)	0.1 (0.03)
3.	3D_1 – resonance at 1.027 MэВ.	$E1$	3P_1	3/2	1611.95103	1.25
	5D_1 - resonance at 1.027 MэВ.	$E1$	5P_1	27/10		
4.	3D_1 - resonance at 4.8 MэВ.	$E1$	3P_1	3/2	4502.245	3.5
	5D_1 - resonance at 4.8 MэВ.	$E1$	5P_1	27/10		
5.	3D_2 - resonance at 4.7 MэВ.	$E1$	3P_1	9/2	6444.382	5.0
	5D_2 - resonance at 4.7 MэВ.	$E1$	5P_1	21/10		

6.	5D_0 - nonresonant scattering wave.	$E1$	5P_1	6/5	800	1.0
7.	3P_2 - resonance at 430 КэВ.	$M1$	3P_1	5/2	11806.017	15.0
	5P_2 - resonance at 430 КэВ.	$M1$	5P_1	9/2		
8.	3P_0 - nonresonant scattering wave.	$M1$	3P_1	2	147.1709	0.18
9.	3P_1 - nonresonant scattering wave.	$M1$	3P_1	3/2	194.68751 (44.70853)	0.22 (0.12)
	5P_1 - nonresonant scattering wave.	$M1$	5P_1	27/2		
10.	3F_3 - resonance at 2.45 МэВ.	$E2$	3P_1	6	5981.83	0.32
	5F_3 - resonance at 2.45 МэВ.	$E2$	5P_1	54/25		
11.	5F_1 - resonance at 1.78 МэВ.	$E2$	5P_1	81/25	5145.881	0.275
12.	5F_1 - resonance at 3.5 МэВ.	$E2$	5P_1	81/25	8787.42	0.47

Cross sections of some $E1$ -transitions, for example, 3, 5 and 6 from the Table 1 can be written as

$$\sigma(E1) = \left\{ \sigma(^3D_1 \rightarrow ^3P_1) + \sigma(^5D_1 \rightarrow ^5P_1) \right\} / 2 + \left\{ \sigma(^3D_2 \rightarrow ^3P_1) + \sigma(^5D_2 \rightarrow ^5P_1) \right\} / 2 + \sigma(^5D_0 \rightarrow ^5P_1)$$

Here, the cross section averaging is performed for the transition from the mixed $D1$ and $D2$ scattering states to the mixed GS. Based on the observables (for resonances this is the state energy and its width), only the potential of $^{3+5}D_1$ or $^{3+5}D_2$ -waves can be built, as well as the $^{3+5}P_1$ -potential for the GS. Therefore, transitions 3 or 5 differ only in the spin coefficients in the expression for the cross section (2), and the matrix elements are calculated between the same WFs mixed along the spin of the channel — this question is described in more detail in [9, 10, 26].

It should be noted here that $M1$ transitions from a $^{3+5}P_1$ scattering wave to the $^{3+5}P_1$ GS in one potential result in zero matrix elements (ME). In other words, if we use the $^{3+5}P_1$ GS potential for the $^{3+5}P_1$ scattering wave, the phase shifts of which are shown in Figure 1a, then the ME of such transitions is zero. At once, we say that in numerical terms, the total cross section for such a transition with the same potential does not exceed $10^{-7} \mu\text{b}$, and the very minimum of the cross sections in our further calculations is of the order of $5 \mu\text{b}$. Further, we use precisely these versions of potentials and this transition 9 makes no real contribution to the total cross sections. Moreover, if we use for a $^{3+5}P_1$ -scattering wave a potential, leading, for example, to zero scattering phase shifts, this transition leads to a value of about $1.5 \mu\text{b}$ at 7 MeV, which gradually increases at zero energy from $0.2 \mu\text{b}$, which is about 1.5% of total cross section at maximum energy. And in this case, the contribution of this transition is small and it does not give a real effect on the

total cross sections.

$n^{11}\text{B}$ interaction potentials

For all partial potentials, i.e. interactions for each orbital moment L at given JS , a Gaussian type with a point Coulomb term was used

$$V(^{2S+1}L_J, r) = -V_0(^{2S+1}L_J) \exp\{-\alpha[^{2S+1}L_J]r^2\},$$

where the depth V_0 and the width α of the potential depend on the momenta $^{2S+1}L_J$ of each partial wave. In some cases, this potential may also depend explicitly on the Young schemes $\{f\}$ and be different in the discrete and continuous spectrum, since in such states these schemes are different [22].

Further, to build the potential of the GS, we note that in [5, 40, 41, 42] for ANC of the form (4) the values from 1.13 to 1.35 fm⁻¹ were obtained, and in [5, 15, 11, 43], the spectrofactor of the GS is given in the range from 0.69 to 1.30. As a result, for the range of dimensional AC we get 0.87 – 1.96 fm⁻¹ or 0.93 – 1.40 fm^{-1/2}, which for the dimensionless AC C_w of the form (6) with $\sqrt{2k_0} = 0.880$ gives an interval of 1.06 – 1.59 with an average value of 1.32 (27).

We now build the potential of the GS with the FS, which correspond to the AC from this range - its parameters are given under No. 9 in the Table 1. This potential gives a negative AC -1.64 (1), because it contains a FS, that is stable in the range of 5 – 17 fm, a charge radius of 2.43 fm and a mass radius of 2.53 fm at a binding energy of -3.37000 MeV with an accuracy of 10⁻⁵ MeV [9, 10, 27], which completely coincides with the experimental value [11]. Hereinafter, the error of the AC is determined by its averaging over a specified distance interval, and the scattering phase shift of this potential is shown in the Figure 1a with a blue solid curve.

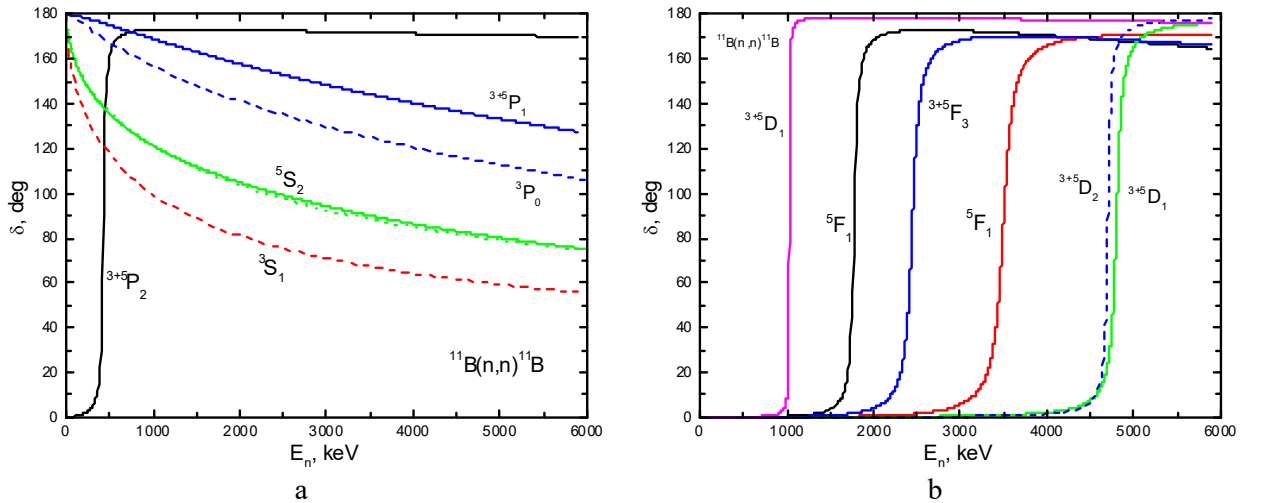


Figure 1. Phase shifts of the elastic $n^{11}\text{B}$ -scattering at low energies obtained using potentials with parameters from the text.

For the third excited 3S_1 -level with an excitation energy of 2.62 MeV or -0.749 MeV relative to the threshold of the $n^{11}\text{B}$ -channel [11], the size of the ANC (with $S_f = 1$) is given in [5, 40, 41] $A_{\text{NC}} = C = 0.94(8)$ fm^{-1/2}. The coefficient $\sqrt{2k_0}$ for this level is 0.605, so for the C_w from (6) we get the interval 1.42 - 1.69 with an average value of 1.55 (14).

In a new paper [44], $S_f = 0.63$ and $A_{NC} = -1.05(5) \text{ fm}^{-1/2}$ are given, then we have $C_w = 2.2(1)$. If we further consider that the AS for the $\{444\}$ scheme in the 3S_1 -wave can be bound and correspond to the third excited state of the ^{12}B nucleus at an energy of -0.7492 MeV relative to the channel threshold, then for the parameters of the 3S_1 -potential without FS, one can get the values given under No. 1 in the Table 1. Using this potential, the binding energy of -0.7492 MeV at $\varepsilon = 10^{-4}$ [27] was found, which fully coincides with the experimental value [11], the charge radius is 2.47 fm , the mass radius equals 2.94 fm and the dimensionless AC equal to $+1.91 (1)$ over the interval $10 - 30 \text{ fm}$. The form of the 3S_1 scattering phase shift with this potential is shown in Figure 1a with a red dashed curve. This potential will be used further to describe the 3S_1 scattering processes and to calculate the first transition under No. 1 of Table 1. The value of its AC is approximately in the middle of the estimated intervals obtained from the data of [5, 40, 41, 44].

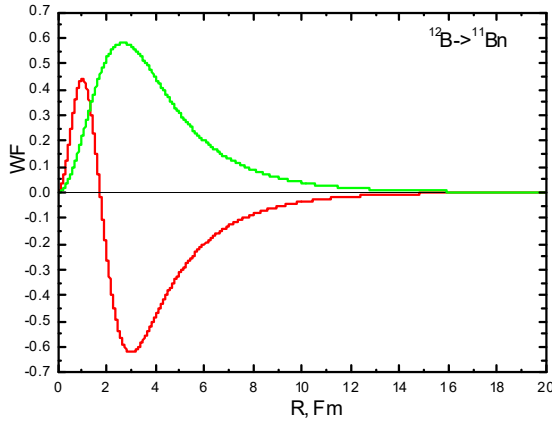


Figure 2a. WF of the ^{12}B nucleus GS in the $n^{11}\text{B}$ channel.

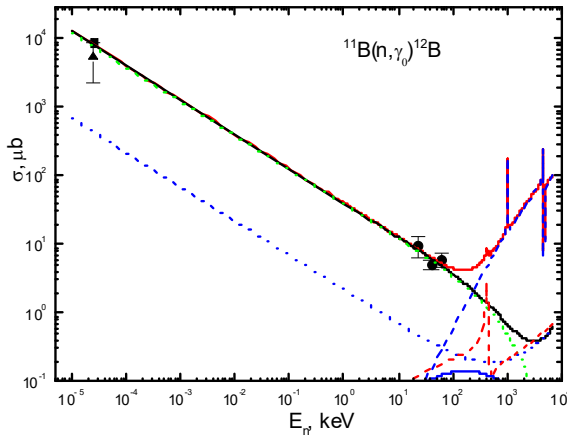


Figure 2b. The total cross sections of the reaction of radiative $n^{11}\text{Be}$ capture for the transition to the GS in the energy range from 10^{-5} keV to 5 MeV . Experimental data: black triangles (▲) - data from [16] at thermal energy, black square (■) - data from [17] at thermal energy, black circles (●) - total cross-sections for the capture on the GS from [45]. Curves are the calculation results for different transitions from Table 1 with the potentials given in the text.

For the second 5S_2 ES, the value $1.34 (12) \text{ fm}^{-1/2}$ (at $S_f = 1$) was obtained in [5, 40, 41], which, at a binding energy of -1.6964 MeV and $\sqrt{2k_0} = 0.742$, gives C_w an interval of $1.64 - 1.97$ with an average of $1.81 (17)$. In a newer paper [44], the values $S_f = 0.33$ and $A_{NC} = -1.28 (6) \text{ fm}^{-1/2}$ are given, then we have $C_w = 3.0 (1)$. In this case, and by analogy with the 3S_1 -wave, for the parameters of this potential you can get the values of No. 2 from the Table 1. This potential leads to a binding energy relative to the channel threshold of -1.6964 MeV , AC equal to $+1.86 (1)$ over the interval $6 - 26 \text{ fm}$, charge radius equals 2.53 fm and mass radius is 2.60 fm . The form of the 5S_2 scattering phase shift with this potential is shown in Figure 1a with a green dotted curve. This potential will be used further to describe the 5S_2 scattering processes and calculate transition No. 2 from Table 1.

This potential has the AC value noticeably less than the results of work [44]; therefore, we consider the second version of this potential No. 2, given in Table 1 in brackets. It leads to the same binding energy, gives the AC equal to $+3.07$, the mass radius is 2.78 fm and the charge radius is 2.45 fm , and its phase shift is shown in Figure 1a with a green continuous curve, which is practically the same as the green dashed curve for the previous potential. However, as will be seen later, its impact on the final results is very small.

It should be noted here that in paper [44] for both S -waves the negative sign of AC is given. For the 3rd ES it is -1.05 (5) $\text{fm}^{-1/2}$ and for the 2nd ES it is -1.28 (6) $\text{fm}^{-1/2}$. The negative sign of AC means the presence of a node in the wave function (WF) of the relative motion of the clusters and the work [44] gives the form of these WFs. However, according to our classification, there are no bound forbidden states in S -waves. According to the classification of states using Young's schemes given below, a bound FS is present only in the P -waves of the discrete spectrum. Therefore, for the GS with potential No. 9 from the Table 1, the AC has a negative sign of -1.64 (1). The WF of this potential is shown in Figure 2a with a red continuous curve. The green continuous curve shows the WF of the GS of the ^{12}B nucleus in the same channel for the potential without a bound FS with the parameters shown in Table 1 No. 9 in brackets. This potential leads to a binding energy of -3.37000 , the same, but positive, AC $+1.64$, mass radius of 2.53 fm, and charge radius of 2.42 fm. The results of the calculation of the total cross sections with this potential and their comparison with the previous potential of the GS will be given below.

For the potential of the resonant $^{3+5}P_2$ -wave with one bound FS, parameters No. 7 were obtained. This potential leads to a resonance energy $E_n = 430$ (1) keV with a width of 37 keV (cm), which completely coincide with the experimental data [11] – for this energy, the scattering phase shift turned out to be 90 (1). To calculate the level width with the scattering phase shift δ the expression $\Gamma = 2(d\delta/dE)^{-1}$ was used, and the form of the resonant mixed $^{3+5}P_2$ scattering phase shift is shown in Figure 1a with the black continuous curve. Recall that the exact mass values of the particles and the \hbar^2/m_0 constant value, that is given above, were used to calculate the scattering phase shifts. These values strongly influence the position of the resonance under consideration or the BS binding energy in the $n^{11}\text{B}$ -channel.

For the potentials of a $^{3+5}P_1$ scattering wave, we will use the potential of the GS No. 9, and for a nonresonant 3P_0 scattering wave with the bound FS, we will use the potential that is matched by the FES, by analogy with the previous ESs No. 1 and No. 2 in the Table 1. Based on the results of [44], where $A_{\text{NC}} = 0.15$ (1) and $S_f = 0.113$ are given, it is possible to obtain with $\sqrt{2k_0} = 0.583$ the dimensionless AC equals 0.77 (2) and potential parameters, which are given under No. 8 in the Table 1. This potential gives a binding energy of -0.6470 MeV, a negative AC $C_w = -0.75$, because it contains FS, the mass radius is 2.75 fm and the charge radius is 2.45 fm. Its scattering phase shift is shown in the Figure 1a with a blue dashed curve.

To consider the $E1$ transitions from a nonresonant 5D_0 scattering wave with a bound FS on the GS, one can use the parameters No. 6 in the Table 1, which lead to the scattering phase shifts less than 0.06° at energies up to 6 MeV in a laboratory system. Here we must remember that if the potential contains $N + M$ forbidden and allowed states, it obeys the Levinson generalized theorem and its phase shift at zero energy begins with $\pi \cdot (N + M)$ [22]. However, in the Figure 1a, the P_1 -phase shift, having a bound FS and a bound FS, is from 180° , not from 360° , and the P_2 -phase shift is from 0 degrees, not from 180° for a more familiar presentation of the results and placement of all phase shifts in one figure. Only the P_0 -phase shift with one bound FS is shown correctly. S -phase shifts, the potentials of which do not have bound FS or AS, are shown from 180° , and not from 0 , for the same reasons. The same comments also apply to the Figure 2b.

For $^{3+5}D_2$, $^{3+5}D_1$ -resonances at 4.7 and 4.8 MeV, respectively, potentials were obtained with the FSs No.5 and No.4. The first of them gives a width of 49 keV, and the second one is of 86 keV, which agrees well with the data [11], and the energies exactly

coincide with those given above. The phase shifts of these potentials are shown in Figure 1b by the blue dashed and green solid curves – at resonance they have a value of $90 (1)^\circ$.

Resonance at 1.027 MeV was also able to be reproduced only under the assumption of the $^{3+5}D_1$ -wave and parameters No. 3 with the FS, which lead to a width of 8.8 keV with exactly the same energy and scattering phase shift, which is shown in Figure 1b with the violet continuous curve, which in resonance is $90 (1)^\circ$.

The resonances at 1.78 and 3.5 MeV could be reproduced only under the assumption of F -waves. In particular, for 5F_1 -waves, the parameters with FS No. 11 and No. 12 are obtained. The first of these gives a width of 56 keV, and the second of 149 keV with exactly the same energy and scattering phase shift shown in Figure 1b with black and red solid curves, which in resonance have values of $90 (1)^\circ$.

The resonance at 2.45 MeV was also able to be reproduced only under the assumption of F -waves. For the $^{3+5}F_3$ -wave, we obtained the parameters with the FS No.10, which lead to a width of 110 keV with exactly the same energy and the scattering phase shifts shown in Figure 1b with the blue solid curve, which has a resonance value of $90 (1)^\circ$.

The $n^{11}\text{B}$ capture total cross sections and reaction rate

The results of the calculation of the total cross sections for the first transition with the scattering potential No. 1 from the Table 1 are shown in Figure 2b by the green dotted curve. These results describe well the experimental data of [17] at the energy of 25.3 meV (black square) and in the region of 23 ± 61 keV (black circles) [45] for the capture on the GS with the potential No. 9 from the Table 1. The cross sections were calculated to a neutron energy up to 7 MeV, but do not take into account resonances above 5 MeV. The blue solid curve in Figure 2 shows the results of calculating the cross section for transition No. 8 from a nonresonant 3P_0 scattering wave to the GS. At the maximum, the magnitude of this cross section is at a level of $0.15 \mu\text{b}$, and the potential of this wave is matched with the AC from [44]. If we use for it the parameters leading to zero scattering phase shifts, the cross section turns out to be much smaller and is not visible in Figure 2.

If we assume that the GS is the $^{3+5}P_1$ mix, then we can consider the second $E1$ -transition under No. 2 from the Table 1, still using potential No. 9 for the GS, which is the potential of the mixed $^{3+5}P_1$ ground state of the ^{12}B in the $n^{11}\text{B}$ -channel. The results of the calculation of the total cross section are shown in the Figure 2b by the blue dotted curve, which leads to the cross sections more than an order of magnitude smaller than the green dotted curve for transition No. 1 from the Table 1. The total cross section for both processes No. 1 is shown in Figure 2 by a black solid curve. If parameters from brackets under No. 2 in Table 1 for the 5S_2 -wave potential are used, which are consistent with the AC data from [44], the result for the sections will differ from the blue dotted curve upwards by about 3%. We will not consider this result here, considering these changes as not significant.

The red dashed curve in the Figure 2b shows the result of calculating the cross sections of the $M1$ capture from the resonant $^{3+5}P_2$ -wave No. 7 from the Table 1. The blue dashed curve shows the $E1$ cross sections with regard to resonances No. 3 at 1027 keV, No. 4, and No. 5 with resonances at 4.7 and 4.8 MeV. The cross sections of resonances No. 10, No. 11, and No. 12 have a very small size and are not visible in the Figure 2b. The red solid curve shows the summarized total cross sections for all the processes listed above.

As can be seen from the Figure 2b, taking into account only transitions from the S -scattering waves allows one to correctly describe the available experimental data in the range from 25 meV to 60 keV. The total cross sections in this energy region are well described by an almost straight line, which at 25 meV agrees with the new data from [17]. The structure of resonances obtained above 400 keV can be considered as a prediction of the results for the total cross sections and a stimulus for new experimental studies of this reaction.

If we use the potential parameters for the ^{12}B GS, shown in brackets under No. 9 in the Table 1, the total cross sections, while retaining their shape, turn out to be an order of magnitude higher. They are no longer able to correctly describe either the data at 25 meV [17] or the measurement results at 20–60 keV from [45]. All resonances are preserved, but they have an order of magnitude or more than the previous results. This value of the total cross sections follows from the shape of the WF of the GS – since the ME is an integral of the WF of scattering and BS, then this integral will be noticeably larger when using the WF shown in the Figure 2a with the green continuous curve.

Since, as can be seen from the Figure 2b, at energies from 10 meV to 10 keV, the calculated cross section is practically a straight line, it can be approximated by a simple function of the form

$$\sigma_{\text{ap}}(\mu\text{b}) = \frac{A}{\sqrt{E(\text{keV})}}.$$

The value of the constant $A = 40.82 \mu\text{b} \cdot \text{keV}^{1/2}$ was determined by one point in the calculated cross sections (red solid curve in the Figure 2b) with a minimum energy of 10 meV. The module

$$M(E) = \left| [\sigma_{\text{ap}}(E) - \sigma_{\text{theor}}(E)] / \sigma_{\text{theor}}(E) \right|$$

of the relative deviation of the calculated theoretical cross section (σ_{theor}) and the approximation (σ_{ap}) of this cross section by the given above function in the region up to 10 keV does not exceed 0.5%.

Further, the reaction rate of the $n^{11}\text{B}$ -capture was calculated, and in units of $\text{cm}^3 \text{mol}^{-1} \text{s}^{-1}$ it can be represented as [28]

$$N_A \langle \sigma v \rangle = 3.7313 \cdot 10^4 \mu^{-1/2} T_9^{-3/2} \int_0^\infty \sigma(E) E \exp(-11.605 E / T_9) dE,$$

where E is given in MeV, the total cross section $\sigma(E)$ is measured in μb , μ is the reduced mass given in a.m.u., and T_9 temperature is given in 10^9 K [28]. To obtain this integral, the calculated total cross section for 7000 points in the energy range from 10^{-5} to $7 \cdot 10^3$ keV was used. A change in this energy range to a larger direction when considering the same processes led to a change in the reaction rate by an amount less than 1%.

For the reaction rate, these results are shown in the Figure 3 – the notation for the curves is similar to the Figure 2b. As can be seen from the Figures 2b and 3, taking into account resonances at an energy of about 5 MeV strongly influences the total cross sections in this area, leading to their large rise, and greatly affects the reaction rate, increas-

ing its value by about 20 times at $10 T_9$. Moreover, this increase is already starting to affect at temperatures above $0.2-0.3 T_9$.

For comparison, a blue solid curve shows the results from [15]. The calculation of this rate was performed taking into account the resonances and, presumably, the capture for all ESs, and the contribution of the direct capture process [15] is shown in the Figure 3 by the blue dash-dotted curve [15], which is generally consistent with our results. A small, approximately one and a half times, excess of our reaction rate over the results of [15] can be explained by the fact that in [15] the cross section was normalized to the data of [16], i.e. to the magnitude of the thermal cross section 5.5 mb. And, as can be seen from the Figure 2b, our calculations describe well the new data for the thermal cross section with a value of 9.09 (10) mb from [17].

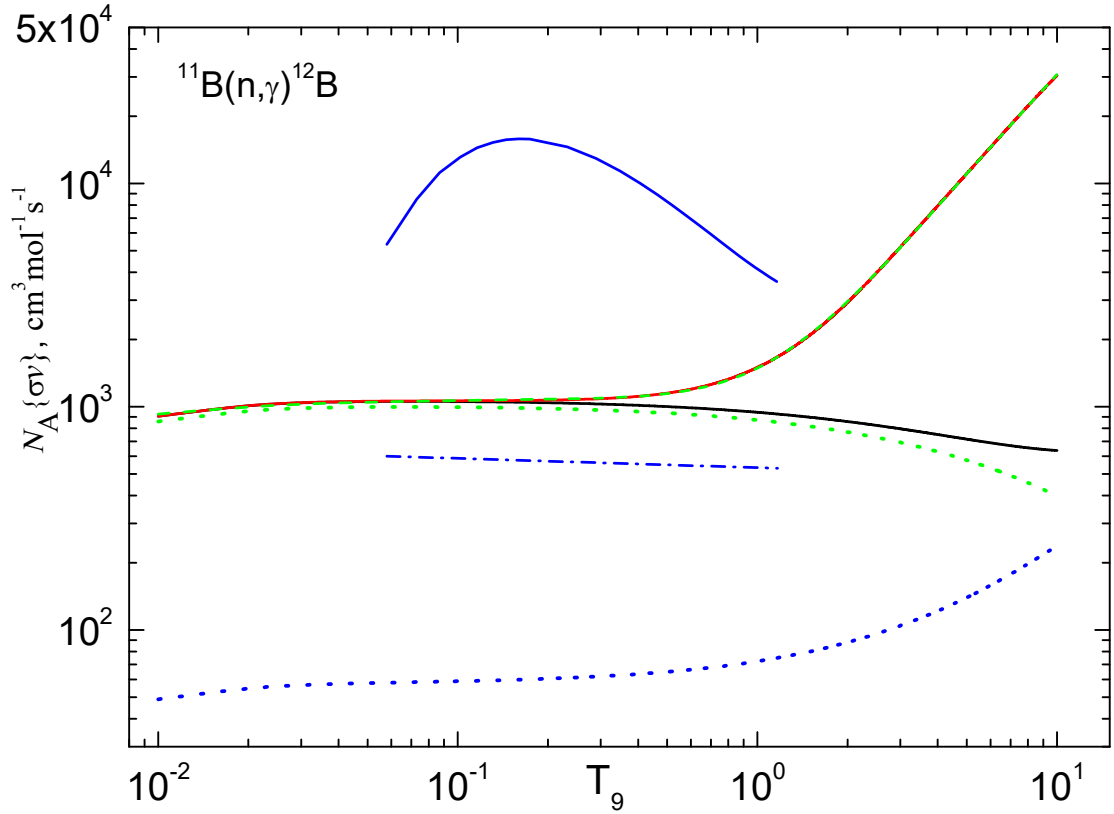


Figure 3. The reaction rate of radiative $n^{11}\text{B}$ -capture at low energies. The designations of the curves, as in Figure 2.

Further, the parameterization of the rate of the reaction was carried out with the parameters given in the Table 2:

$$N_A \langle \sigma v \rangle = a_1 / T_9^{2/3} \cdot \exp(-a_2 / T_9^{1/3}) \cdot (1.0 + a_3 \cdot T_9^{1/3} + a_4 \cdot T_9^{2/3} + a_5 \cdot T_9 + a_6 \cdot T_9^{4/3} + a_7 \cdot T_9^{5/3})$$

Table 2. Parameters of the analytical parametrization of the reaction rate.

N_0	a_i
1.	34.15923
2.	0.39497
3.	56.25945
4.	-214.8073

5.	611.29
6.	-717.15
7.	328.18
$\chi^2 = 0.008$	

The results of that parameterization are shown in the Figure 3 by the green dashed curve, the value $\chi^2 = 0.008$ with 5% error of the calculated reaction rate.

Conclusion

So, the results of our calculations for the total cross sections of the $n^{11}\text{B}$ -capture on the GS are in good agreement with the available experimental data from [17, 45] in the energy range from 10^{-5} and approximately to 10^2 keV. The GS potential of the ^{12}B nucleus in the $n^{11}\text{B}$ -channel is preliminarily matched with its characteristics, including the asymptotic constant and binding energy, and for the S and P_0 -scattering potentials, the interactions of the second, third, and fourth excited states of ^{12}B bound in the $n^{11}\text{B}$ -channel are used.

Taking into account the resonances up to 5 MeV increases the total cross sections in this energy region by approximately two orders of magnitude relative to the results for capture only from S -waves. The reaction rate at a temperature of more than $0.2\text{-}0.3 T_9$ starts to increase and increases about 20 times at $10 T_9$. As far as we know, such results for the reaction rate were obtained for the first time. They can significantly affect the result of calculations of the yield of the ^{12}B nucleus in the primordial nucleosynthesis at high temperatures.

In conclusion, it should be noted that the new work on the processing of experimental data on the $^{11}\text{B}(d,p)^{12}\text{B}$ reaction [44] provides data on the ANC for the four bound ESs of the ^{12}B nucleus. This information is promising for further calculations of the characteristics of the synthesis of ^{12}B in the reaction of radiative neutron capture on the ^{11}B nucleus during the capture of the all ESs of the final nucleus. This probably may lead to a revision of certain astrophysical results on the reaction rate.

Acknowledgements

This work was supported by the Grant of Ministry of Education and Science of the Republic of Kazakhstan through the program BR05236322 “Study reactions of thermonuclear processes in extragalactic and galactic objects and their subsystems” in the frame of theme “Study of thermonuclear processes in stars and primordial nucleosynthesis” through the Fesenkov Astro-physical Institute of the National Center for Space Research and Technology of the Ministry of Defence and Aerospace Industry of the Republic of Kazakhstan (RK).

References

1. Heil M. et al. The (n,γ) cross section of ^7Li // *Astrophys. Jour.* 1998. V.507. P.997-1002.
2. Nagai Y. et al. Fast neutron capture reactions in nuclear astrophysics // *Hyperfine Interactions* 1996. V.103. P.43-48.
3. Masayuki Igashira, Toshiro Ohsaki Neutron capture nucleosynthesis in the Uni-

verse // Sci. Tech. Adv. Materials 2004. V.5. P.567-573.

4. Guimaraes V. and Bertulani C.A. Light radioactive nuclei capture reactions with phenomenological potential models // AIP Conf. Proc. 2010. V.1245. P.30-38; <https://arxiv.org/abs/0912.0221>.

5. Liu Z.H. et al. Asymptotic normalization coefficients and neutron halo of the excited states in ^{12}B and ^{13}C // Phys. Rev. 2001. V.C64. P.034312(1- 5).

6. Dubovichenko S.B., Burkova N.A., Dzhazairov-Kakhramanov A.V., Tkachenko A.S. New results for neutron radiative capture on ^{10}Be at energies between 25.3 meV to 10.0 MeV // Astropart. Phys. 2019. V.104. P.91-101.

7. Dubovichenko S.B., Burkova N.A., Dzhazairov-Kakhramanov A.V. Influence of low-lying resonances on reaction rates for $n^{10}\text{B}$ capture // [arXiv:1904.09069v1](https://arxiv.org/abs/1904.09069v1) [nucl-th].

8. Dubovichenko S.B., Burkova N.A., Dzhazairov-Kakhramanov A.V., Tkachenko A.S. New result for the $p^7\text{Be} \rightarrow ^8\text{B}\gamma$ astrophysical S -factor from 10 keV to 5 MeV and reaction rate from 0.01 to 10 T_9 // Nucl. Phys. 2019. V.A983. P.175-194.

9. Dubovichenko S.B. Thermonuclear processes in Stars and Universe. Second English Edition, revised and expanded. Germany, Saarbrücken: Scholar's Press. 2015. 332p.; <https://www.scholars-press.com/catalog/details/store/gb/book/978-3-639-76478-9/Thermonuclear-processes-in-stars>.

10. Dubovichenko S.B. Radiative neutron capture. Primordial nucleosynthesis of the Universe. First English edition. Germany. Berlin. deGruyter 2019. 293p. ISBN 978-3-11-061784-9. <https://doi.org/10.1515/9783110619607-201>

11. Kelley J.H., Purcell J.E., Sheu C.G. Energy level of light nuclei $A=12$ // Nucl. Phys. 2017. V. A968. P.71-253.

12. Dubovichenko S.B., Dzhazairov-Kakhramanov A.V., Burkova N.A., Tkachenko A.S. Neutron capture on ^{11}B and ^{12}B at astrophysical energies // Russ. Phys. Jour. 2017. V.60. P.666-677.

13. Ajzenberg-Selove F. Energy level of light nuclei $A=11,12$ // Nucl. Phys. 1990. V.A506. P.1-158.

14. <http://cdfc.sinp.msu.ru/exfor/index.php>

15. Lee H.Y. et al. Experimental study of the $^{11,12}\text{B}(n,\gamma)$ reactions and their influence on r-process nucleosynthesis of light elements // Phys. Rev. 2010. V.C81. P.015802.

16. Mughabghab S.F. Atlas of neutron resonances. National Nuclear Data Center. Brookhaven. National Laboratory. Upton, USA 2006. 1008p.

17. Firestone R.B., Revay Zs. Thermal neutron radiative cross sections for $^{6,7}\text{Li}$, ^9Be , $^{10,11}\text{B}$, $^{12,13}\text{C}$, and $^{14,15}\text{N}$ // Phys. Rev. 2016. V.C93. P.054306.

18. Wildermut K., Tang Y.C. A unified theory of the nucleus. Branschweig: Vieweg. 1977. 498p.

19. Mertelmeir T., Hofmann H.M. Consistent cluster model description of the electromagnetic properties of lithium and beryllium nuclei // Nucl. Phys. 1986. V.A459. P.387.

20. Descouvemont P., Dufour M. Microscopic cluster model // In: Clusters in Nuclei. V.2. Editor C. Beck. Berlin-Heidelberg: Springer-Verlag. 2012. 353p.

21. Nesterov A.V. et al. Three clusters description of light nuclei properties // Phys. Part. Nucl. 2010. V.41. №5. P.716-765.

22. Neudatchin V.G. et al. Generalized potential model description of mutual scattering of the lightest $p^2\text{H}$, $^2\text{H}^3\text{He}$ nuclei and the corresponding photonuclear reactions // Phys. Rev. 1992. V.C45. P.1512-1527.

23. Nemets O.F. et al. Nucleon Association in Atomic Nuclei and the Nuclear Reac-

- tions of the Many Nucleons Transfers. Kiev: Nauk. Dumka, 1988. 488p. (in Russian).
24. Dubovichenko S.B., Dzhazairov-Kakhramanov A.V. Study of the Nucleon Radiative Captures $^8\text{Li}(n,\gamma)$, $^9\text{Be}(p,\gamma)$, $^{10}\text{Be}(n,\gamma)$, $^{10}\text{B}(p,\gamma)$, and $^{16}\text{O}(p,\gamma)$ at Thermal and Astrophysical Energies // Int. Jour. Mod. Phys. 2017. V.E25. №3. P.1630009 (56p.).
 25. Dubovichenko S.B., Dzhazairov-Kakhramanov A.V. The radiative $^{10}\text{Be}(n,\gamma)^{11}\text{Be}$ capture at thermal and astrophysical energies // J. Phys. 2016. V.G43. №9. P.095201(14p.).
 26. Dubovichenko S.B., Dzhazairov-Kakhramanov A.V. The reaction $^8\text{Li}(n,\gamma)^9\text{Li}$ at astrophysical energies and its role in primordial nucleosynthesis // AstroPhys. J. 2016. V.819. №1. P.78(8p.).
 27. Dubovichenko S.B., Dzhazairov-Kakhramanov A.V. Thermonuclear processes for three-nucleon systems in potential cluster model // Nucl. Phys. 2015. V.A941. P.335-363.
 28. Angulo C. et al. A compilation of charged-particle induced thermonuclear reaction rates // Nucl. Phys. 1999. V.A656. P.3-183.
 29. Dubovichenko S.B., Dzhazairov-Kakhramanov A.V. Photonuclear processes on ^7Li and ^7Be in the cluster model for potentials with forbidden states // Phys. Atom. Nucl. 1995. V.58. P.579-585.
 30. Dubovichenko S.B., Dzhazairov-Kakhramanov A.V. Electromagnetic effects in light nuclei and the cluster potential model // Phys. Part. Nucl. 1997. V.28. №6. P.615-641.
 31. http://physics.nist.gov/cgi-bin/cuu/Value?mud|search_for=atomnuc!
 32. http://cdfc.sinp.msu.ru/services/ground/NuclChart_release.html
 33. Mukhamedzhanov A.M., Tribble R.E. Connection between asymptotic normalization coefficients, sub threshold bound states, and resonances // Phys. Rev. 1999. V.C59. P.3418-3424.
 34. Hodgson P.E. The Optical model of elastic scattering. Oxford: Clarendon Press. 1963. 211p.
 35. Plattner G.R., Viollier R.D. Coupling constants of commonly used nuclear probes // Nucl. Phys. 1981. V.A365. P.8.
 36. Itzykson C., Nauenberg M. Unitary groups: Representations and decompositions // Rev. Mod. Phys. 1966. V.38. P.95.
 37. Dubovichenko S.B., Dzhazairov-Kakhramanov A.V., Afanasyeva N.V. Neutron radiative capture by ^9Be , ^{14}C , ^{14}N , ^{15}N and ^{16}O at astrophysical energies // Int. Jour. Mod. Phys. 2013. V.E22. P.1350075(53p.).
 38. Dubovichenko S.B., Dzhazairov-Kakhramanov A.V., Burkova N.A. Neutron radiative capture by ^2H , ^6Li , ^7Li , ^{12}C and ^{13}C at astrophysical energies // Int. Jour. Mod. Phys. 2013. V.E22. №5. P. 1350028(52p.).
 39. Dubovichenko S.B., Dzhazairov-Kakhramanov A.V., Burkova N.A. New theoretical results for radiative $^3\text{H}(p,\gamma)^4\text{He}$, $^3\text{He}(^2\text{H},\gamma)^5\text{Li}$, $^4\text{He}(^2\text{H},\gamma)^6\text{Li}$, $^4\text{He}(^3\text{H},\gamma)^7\text{Li}$ and $^4\text{He}(^3\text{He},\gamma)^7\text{Be}$ captures at astrophysical energies // Int. Jour. Mod. Phys. 2019. V.E28. №3. P.1930004(49p.).
 40. Lin Cheng-Jian et al. Excitation Halo States of ^{12}B // Chin. Phys. Lett. 2001. V.18, No.9. P.1183-1185.
 41. Guo B. et al. Determination of astrophysical $^{11}\text{C}(p,\gamma)^{12}\text{N}$ reaction rate from the asymptotic normalization coefficients of $^{12}\text{B} \rightarrow ^{11}\text{B} + n$ // J. Phys. G: Nucl. Part. Phys. 2007. V. 34. P.103–114.
 42. Timofeyuk N.K. Spectroscopic factors and asymptotic normalization coefficients

for 0 p-shell nuclei: Recent updates // Phys. Rev.2013. V.C88. P.044315.

43. Cook J., Stephens M.N. and Kemper K.W. Elastic scattering and single nucleon transfer reactions for ${}^7\text{Li} + {}^{11}\text{B}$ and ${}^7\text{Li} + {}^{13}\text{C}$ at 34 MeV // Nucl. Phys. 1987. V.A466. P.168-188.

44. Belyaeva L.T. et al. Neutron halos in the excited states of ${}^{12}\text{B}$ // Phys. Rev. 2018. V.C98. P.034602(10p.).

45. Igashira M. et al. Measurements of keV-neutrons capture gamma rays // Conf. Meas. Calc. and Eval. of Photon Prod. Data. Bologna. 1964. P.269.

46. Caughlan G.R., Fowler W.A. // Atom. Data Nucl. Data Tab. 1988. V.40. P.283-334.